Journal of Solid State Chemistry 183 (2010) 2004–2011

Contents lists available at ScienceDirect

Journal of Solid State Chemistry

journal homepage: www.elsevier.com/locate/jssc

Controlled synthesis and luminescent properties of $Eu^{2+}(Eu^{3+})$, Dy^{3+}-doped $Sr_3Al_2O_6$ phosphors by hydrothermal treatment and postannealing approach

Xiang Ying Chen [a,*], Shi Ping Bao [a], Yu Cheng Wu [b]

[a] School of Chemical Engineering, Anhui Key Laboratory of Controllable Chemistry Reaction & Material Chemical Engineering, Hefei University of Technology, Hefei, Anhui 230009, P.R. China
[b] School of Materials Science and Engineering, Hefei University of Technology, Hefei, Anhui 230009, P.R. China

ARTICLE INFO

Article history:
Received 28 January 2010
Received in revised form
7 April 2010
Accepted 9 April 2010
Available online 13 April 2010

Keywords:
$Sr_3Al_2O_6$
Phosphor
Hydrothermal
Postannealing

ABSTRACT

In this work, $Sr_3Al_2O_6$: Eu^{2+} (Eu^{3+}), Dy^{3+} phosphors have been prepared by hydrothermal treatment and subsequently postannealing approach, using $Sr(NO_3)_2$, $Al(NO_3)_3 \cdot 9H_2O$, and $CO(NH_2)_2$ as starting materials. The as-obtained phosphors were characterized by means of XRPD, FESEM, and PL techniques. In addition, many reaction parameters were studied in detail, including the initial mole ratios, hydrothermal reaction temperature, calcination temperature and calcination atmosphere. Remarkably, two scientific merits exist herein: $Sr_3Al_2O_6$: Eu^{2+} (Eu^{3+}), Dy^{3+} phosphors can be selectively obtained in a reducing atmosphere (H_2/Ar, 20%+80%) and in air, respectively; adding certain amount of sodium citrate can alter the shape and size of $Sr_3Al_2O_6$: Eu^{2+} (Eu^{3+}), Dy^{3+} phosphors in essence. Besides, the luminescent properties of $Sr_3Al_2O_6$: Eu^{2+} (Eu^{3+}), Dy^{3+} phosphors were studied by excitation spectra, emission spectra and decay curves.

1. Introduction

Inorganic phosphors doped with rare earth ions have attracted extensive attention thanks to their remarkable luminescent properties and applications, commonly referring as of lamp industry, radiation dosimetry, X-ray imaging, and color display [1–3]. Compared with sufide-based phosphors, the europium-doped strontium aluminates exhibit lots of merits such as good stability [4], long persistence, and high quantum efficiency [5].

As an efficient red luminescent activator, trivalent europium (Eu^{3+}) is widely utilized because of the electronic transitions from the lowest $^5D_0$ excited state to ^7F_J (J=0, 1, 2, 3, 4) ground state, which strongly depend on their local environments in host lattices [6,7]. On the other hand, Eu^{2+}-doped phosphors can reveal intense broad-band emissions, deriving from the electronic transitions between the ground state of $4f^7$ and the excited state of $4f^65d^1$ of Eu^{2+} ions. Besides, to enhance the initial intensity of luminescence and afterglow of europium-doped phosphors, a certain amount of Ln^{3+} co-activators (most commonly as Dy, Nd) are added, which can result in prominent increase on them [8].

In the SrO–Al_2O_3 system, many stoichiometric compounds exist, such as $Sr_3Al_2O_6$ [9], $SrAl_2O_4$ [10–12], $Sr_4Al_4O_{25}$ [13], $SrAl_4O_7$ and $SrAl_{12}O_{19}$ [14]. Typically, these aluminates were prepared by solid-state reaction of mechanically mixed powders ($SrCO_3$ and Al_2O_3), which requires rigorous operation conditions and compositional inhomogeneity inevitably occurs. To avoid the above disadvantages involved in solid-state method, many alternative preparative methods were put forward as yet. Taking sol-gel method as an example, Xu and co-workers prepared $Sr_3Al_2O_6$ powders by calcining citric acid precursor at a temperature of 900–1200 °C [15].

Recently, we prepared a series of necklace-like MAl_2O_4:Eu^{2+}, Dy^{3+} (M=Sr, Ba, Ca) phosphors via a CTAB-assisted solution-phase synthesis and postannealing approach [16], which can provide us a gentler method to prepare aluminate phosphors. As the extension of this work, we herein prepared $Sr_3Al_2O_6$ phosphors doped with Eu^{2+}(Eu^{3+}), Dy^{3+} by hydrothermal treatment and subsequently postannealing approach. Firstly, $Sr(NO_3)_2$, $Al(NO_3)_3 \cdot 9H_2O$, and $CO(NH_2)_2$ with various mole ratios were hydrothermally treated to prepare white powders acting as precursor, which were further calcined at 1200 °C for 3 h. The luminescent properties of $Sr_3Al_2O_6$: Eu^{2+} (Eu^{3+}), Dy^{3+} phosphors were studied by excitation spectra, emission spectra and decay curves. In this work, many scientific merits clearly appear as follows: (1) $Sr_3Al_2O_6$: Eu^{2+} (Eu^{3+}), Dy^{3+} phosphors can be selectively obtained in a reducing atmosphere (H_2/Ar, 20%+80%) and in air, respectively; (2) adding certain amount of sodium citrate can alter the shape and size of $Sr_3Al_2O_6$: Eu^{2+} (Eu^{3+}), Dy^{3+} phosphors in essence.

2. Experimental section

All the chemicals are of analytical grade and used as received without further purification. In this work, a series of contrast

* Corresponding author. Fax: +86 551 2901450.
E-mail address: cxyhfut@gmail.com (X.Y. Chen).

0022-4596/$ - see front matter © 2010 Elsevier Inc. All rights reserved.
doi:10.1016/j.jssc.2010.04.008

experiments were carried out by adjusting the initial mole ratios of $Sr(NO_3)_2$, $Al(NO_3)_3 \cdot 9H_2O$, and $CO(NH_2)_2$ (3:2:20, 3:2:30, 3:2:40, and 3:2:50), calcination temperatures (900, 1000, 1100, and 1200 °C) and calcination atmospheres (in a reducing atmosphere of H_2/Ar and in air). Besides, spherical $Sr_3Al_2O_6$:Eu^{3+}, Dy^{3+} phosphors were obtained by adding certain amounts of sodium citrate (10, 20, and 30 mmol).

2.1. Preparing the precursor of $Sr_3Al_2O_6$: Eu^{2+}, Dy^{3+} phosphor via hydrothermal route

$Sr(NO_3)_2$ (9 mmol), $Al(NO_3)_3 \cdot 9H_2O$ (6 mmol), $CO(NH_2)_2$ (20 mmol), $Eu(NO_3)_3$ (0.02 mmol), and $Dy(NO_3)_3$ (0.03 mmol) were in turn dissolved in 40 mL distilled H_2O under magnetic stirring. The above solution was then transferred into a 50 mL Teflon-lined stainless steel autoclave, which was then sealed and kept at 120 °C. After 12 h, the resulting fluffy white product was filtered off, washed with distilled water and absolute ethanol for several times, and then dried under vacuum at 60 °C for 6 h.

2.2. Preparing the $Sr_3Al_2O_6$: Eu^{2+}, Dy^{3+} phosphor via postannealing approach

The final $Sr_3Al_2O_6$: Eu^{2+}, Dy^{3+} phosphor was obtained in an electric furnace by postannealing the precursor at 1200 °C for 3 h in a reducing atmosphere of H_2/Ar (20%+80%).

Regarding $Sr_3Al_2O_6$: Eu^{3+}, Dy^{3+} phosphor, the preparative procedure is similar to the aforementioned procedure for $Sr_3Al_2O_6$: Eu^{2+}, Dy^{3+} phosphor, except for substituting the reducing atmosphere of H_2/Ar with air.

2.3. Characterization

X-ray powder diffraction (XRPD) patterns were obtained on a Rigaku Max-2200 with Cu$K\alpha$ radiation. Field emission scanning electron microscopy (FESEM) images were taken with a Hitachi S-4800 scanning electron microscope. Photoluminescent (PL) analysis was conducted on a Hitachi F-4500 spectrophotometer with Xe lamp at room temperature.

3. Results and discussion

X-ray powder diffraction (XRPD) technique is an effective tool to determine the phase, crystallinity and purity of samples prepared under various conditions. We first investigated the reaction system containing $Al(NO_3)_3 \cdot 9H_2O$, $Sr(NO_3)_2$, $CO(NH_2)_2$ as the starting materials with various mole ratios of 3:2:20, 3:2:30, 3:2:40, and 3:2:50. When the above starting materials were treated in the mole ratio of 3:2:20 at 120 °C for 12 h, white fluffy products were formed. The corresponding XRPD pattern is shown in Fig. 1a, which indicates that the precursor is composed of orthorhombic $NH_4Al(OH)_2CO_3$ (JCPDS Card No.42-0250) and orthorhombic $SrCO_3$ (JCPDS Card No.05-0418). Next, when increasing the mole ratio of $Al(NO_3)_3 \cdot 9H_2O$, $Sr(NO_3)_2$, $CO(NH_2)_2$ up to 3:2:30, 3:2:40, or 3:2:50, the resulting XRPD patterns are

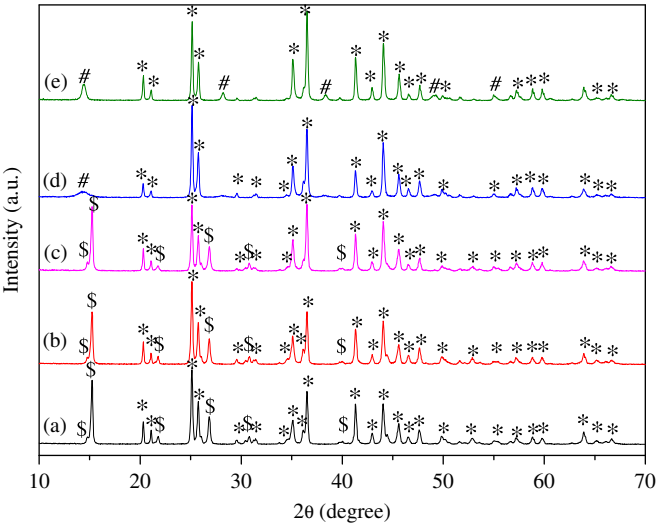

Fig. 2. XRPD patterns of samples acting as precursors obtained by keeping the mole ratio of $Sr(NO_3)_2$, $Al(NO_3)_3 \cdot 9H_2O$, and $CO(NH_2)_2$ as 3:2:20 at various reaction temperatures for 12 h: (a) 120 °C, (b) 140 °C, (c) 160 °C, (d) 180 °C, and (e) 200 °C. *=orthorhombic $SrCO_3$ (JCPDS Card No.05-0418), ♯=orthorhombic γ–AlOOH (JCPDS Card No.21-1307), $=orthorhombic $NH_4Al(OH)_2CO_3$ (JCPDS Card No.42-0250).

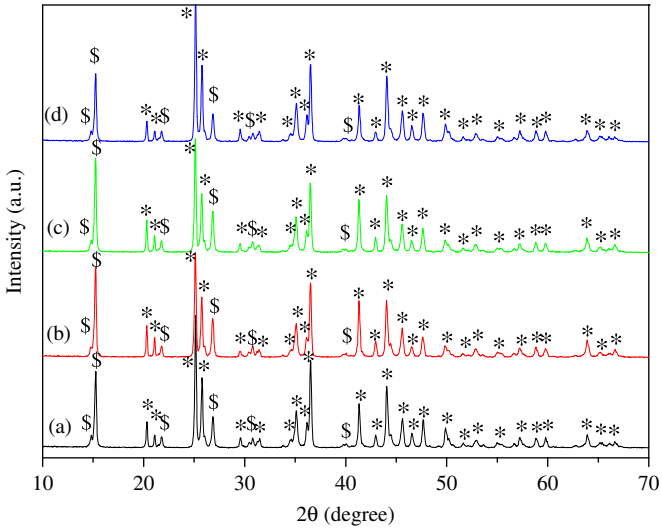

Fig. 1. XRPD patterns of samples acting as precursors obtained by hydrothermal treatment of $Sr(NO_3)_2$, $Al(NO_3)_3 \cdot 9H_2O$, and $CO(NH_2)_2$ at 120 °C for 12 h with various mole ratios: (a) 3:2:20, (b) 3:2:30, (c) 3:2:40, and (d) 3:2:50. $=orthorhombic $NH_4Al(OH)_2CO_3$ (JCPDS Card No.42-0250), *=orthorhombic $SrCO_3$ (JCPSDS Card No.05-0418).

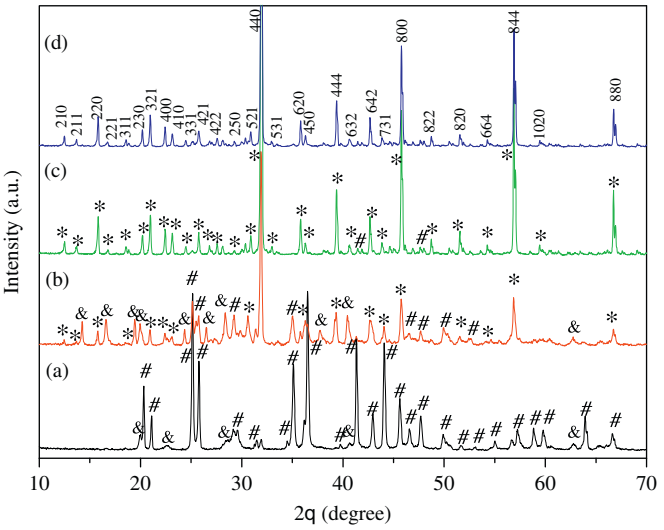

Fig. 3. XRPD patterns of samples obtained by calcining the precursor prepared at 120 °C for 12 h by keeping the mole ratio of $Sr(NO_3)_2$, $Al(NO_3)_3 \cdot 9H_2O$, and $CO(NH_2)_2$ as 3:2:20 at various calcination temperatures in air for 3 h: (a) 900 °C, (b) 1000 °C, (c) 1100 °C, and (d) 1200 °C. *=cubic $Sr_3Al_2O_6$ (JCPDS Card No.24-1187), ♯=orthorhombic $SrCO_3$ (JCPDS Card No.05-0418), &=unidentified phases.

shown in Fig. 1b–d. To our surprise, those XRPD patterns are almost the same as that shown in Fig. 1a, regardless of the mole ratio of starting materials. Considering the cost of preparation for precursor, we chose the optimal mole ratio of $Al(NO_3)_3 \cdot 9H_2O$, $Sr(NO_3)_2$, $CO(NH_2)_2$ as 3:2:20.

Fig. 2 shows the XRPD patterns of the samples obtained by keeping the mole ratio of $Sr(NO_3)_2$, $Al(NO_3)_3 \cdot 9H_2O$, and $CO(NH_2)_2$ as 3:2:20 at various reaction temperatures for 12 h. When conducting the experiment at 120 °C for 12 h, the corresponding XRPD pattern is given in Fig. 2a, which consists of orthorhombic $NH_4Al(OH)_2CO_3$ (JCPDS Card No.42-0250) and orthorhombic $SrCO_3$ (JCPDS Card No.05-0418). Next, when increasing the reaction temperature to 140 or 160 °C, the resulting XRPD patterns in Fig. 2b,c are analogous to that obtained at 120 °C. Remarkably, when conducting the experiment at 180 °C or 200 °C for 12 h, some diffraction peaks assignable to orthorhombic γ–AlOOH (JCPDS Card No.21-1307) appear in Fig. 2d,e, together with orthorhombic $SrCO_3$ (JCPDS Card No.05-0418). From Fig. 2, we can see that the higher reaction temperature is in favor of the formation of γ–AlOOH under present hydrothermal conditions. This viewpoint is, to some extent, in accordance with our previous research results in which γ–AlOOH nanoplatelets and nanowires were controllably synthesized under basic and acidic circumstances, respectively. In particular, we found that the higher reaction temperature, the better crystallinity in nature towards γ–AlOOH nanocrystals [17]. In addition, considering the cost of preparation for precursor, we chose the hydrothermal conditions as 120 °C for 12 h.

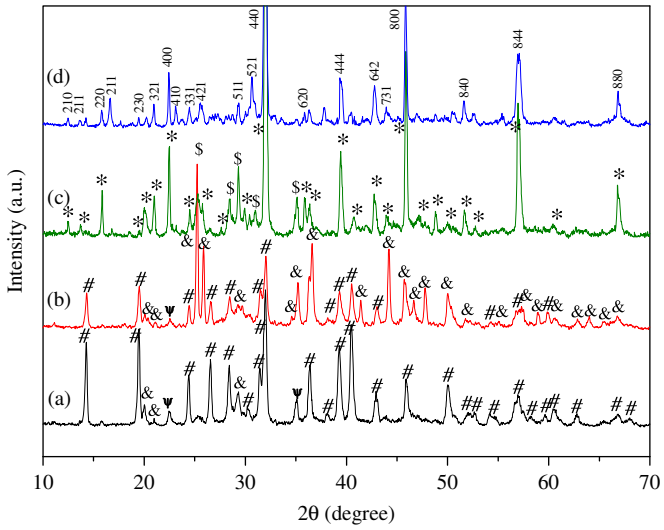

Fig. 4. XRPD patterns of samples obtained by calcining the precursor prepared at 120 °C for 12 h by keeping the mole ratio of $Sr(NO_3)_2$, $Al(NO_3)_3 \cdot 9H_2O$, and $CO(NH_2)_2$ as 3:2:20 at various calcination temperatures in a reducing atmosphere of H_2/Ar (20%+80%) for 3 h: (a) 900 °C, (b) 1000 °C, (c) 1100 °C, and (d) 1200 °C. ♯=$Sr(OH)_2 \cdots H_2O$ (JCPDS Card No.22-1222), ✻=cubic $Sr_3Al_2O_6$ (JCPDS Card No.24-1187), &=orthorhombic $SrCO_3$ (JCPDS Card No.05-0418), $=monoclinic $SrAl_2O_4$ (JCPDS Card No.34-0379), Ψ=unidentified phases.

To obtain the final $Sr_3Al_2O_6$: Eu^{3+}, Dy^{3+} product, the above precursor hydrothermally prepared at 120 °C for 12 h by keeping the mole ratio of $Sr(NO_3)_2$, $Al(NO_3)_3 \cdot 9H_2O$, and $CO(NH_2)_2$ as 3:2:20 was further calcined in air at various calcination temperatures ranging from 900 to 1200 °C. Fig. 3a shows the typical XRPD pattern of the product obtained in air at 900 °C for 3 h, which mainly consists of orthorhombic $SrCO_3$ (JCPDS Card No.05-0418) as well as minor unidentified phases. When increasing the calcination temperature to 1000 °C, lots of diffraction peaks indexed as cubic $Sr_3Al_2O_6$ (JCPDS Card No. 24-1187) occur, as shown in Fig. 3b. To enhance the crystallinity and purity of samples, elevated reaction temperature is commonly employed. As a result, $Sr_3Al_2O_6$: Eu^{3+}, Dy^{3+} phosphor was obtained at 1200 °C for 3 h in air.

Next, in order to prepare $Sr_3Al_2O_6$: Eu^{2+}, Dy^{3+} phosphor, we conducted the experiments in a reducing atmosphere of H_2/Ar (20%+80%) while keep other parameters unchanged as mentioned for $Sr_3Al_2O_6$: Eu^{3+}, Dy^{3+} phosphor. When calcining the precursor at 900 °C or 1000 °C for 3 h, the resulting products are mainly composed of $Sr(OH)_2 \cdot H_2O$ (JCPDS Card No.22-1222) and orthorhombic $SrCO_3$ (JCPDS Card No.05-0418), together with minor unidentified phases, as shown in Fig. 4a,b. When further increasing the calcination temperature to 1100 °C, cubic

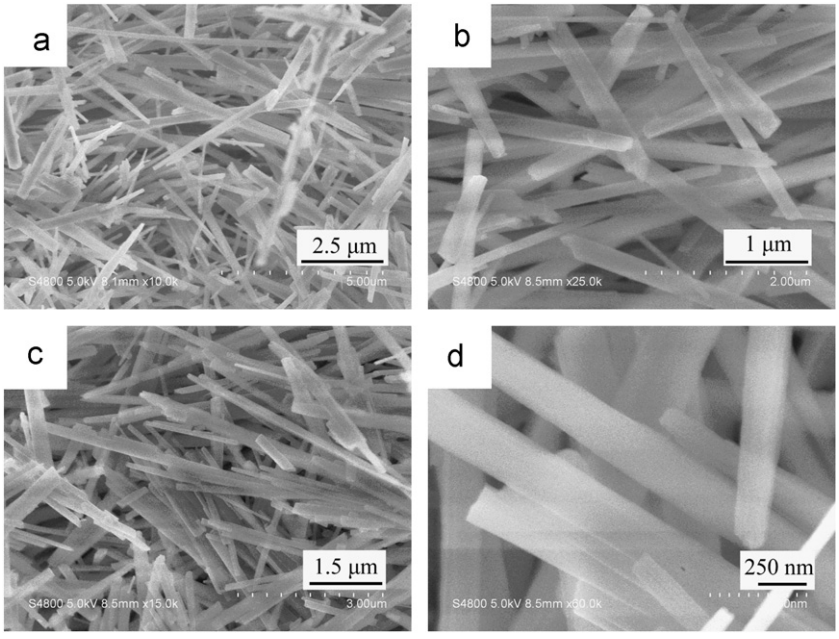

Fig. 5. FESEM images of samples acting as precursors obtained by hydrothermal treatment of $Sr(NO_3)_2$, $Al(NO_3)_3 \cdot 9H_2O$, and $CO(NH_2)_2$ at 120 °C for 12 h with various mole ratios: (a) 3:2:20, (b) 3:2:30, (c) 3:2:40, and (d) 3:2:50.

$Sr_3Al_2O_6$ (JCPDS Card No.24-1187) as major phase together with minor monoclinic $SrAl_2O_4$ (JCPDS Card No.34-0379) appear, as revealed in Fig. 4c. Finally, we obtained the pure phase $Sr_3Al_2O_6$: Eu^{2+}, Dy^{3+} phosphor at 1200 °C for 3 h in a reducing atmosphere of H_2/Ar (20%+80%), accompanying with the vanishing of monoclinic $SrAl_2O_4$.

FESEM technique has been proved to be a powerful tool to vividly illustrate the sizes and shapes of samples. Fig. 5 demonstrates the representative FESEM images of the precursor obtained by hydrothermal treatment of $Sr(NO_3)_2$, $Al(NO_3)_3 \cdot 9H_2O$, and $CO(NH_2)_2$ at 120 °C for 12 h with various mole ratios. When setting the mole ratio of $Sr(NO_3)_2$, $Al(NO_3)_3 \cdot 9H_2O$, and $CO(NH_2)_2$ as 3:2:20, the resulting sample is mainly composed of 1-D nanostructures with the diameters of hundreds of nanometers and lengths up to tens of micrometers, as shown in Fig. 5a. As for the cases of mole ratios of $Sr(NO_3)_2$, $Al(NO_3)_3 \cdot 9H_2O$, and $CO(NH_2)_2$ as 3:2:30, 3:2:40, and 3:2:50, the sizes and shapes of the corresponding samples in Fig. 5b–d are almost the same to that shown in Fig. 5a. Moreover, the surfaces of the as-obtained nanowires are quite smooth and defect-free, clearly demonstrated by Fig. 5d. Consequently, we find out that the initial mole ratio of $Sr(NO_3)_2$, $Al(NO_3)_3 \cdot 9H_2O$, and $CO(NH_2)_2$ involved herein can hardly affect the size and shape of the products.

Besides, the sizes and shapes of the samples obtained by keeping the mole ratio of $Sr(NO_3)_2$, $Al(NO_3)_3 \cdot 9H_2O$, and $CO(NH_2)_2$ as 3:2:20 at various reaction temperatures were investigated based on FESEM technique. In terms of the FESEM images in Fig. 6a–d, we can see that the as-prepared samples at 120, 140, and 160 °C for 12 h are nearly equal in size and shape, composing of large numbers of 1-D nanostructures, which well accords with the FESEM results shown in Fig. 5. These results are also consistent with the XRPD patterns in Fig. 2a–c, whose resultant products all consist of orthorhombic $NH_4Al(OH)_2CO_3$ and orthorhombic $SrCO_3$ in substance. On the other hand, we can see in Fig. 2d,e that some diffraction peaks indexed as orthorhombic γ–AlOOH appear when conducting the experiment at 180 °C or 200 °C for 12 h, probably resulting in the discrepancy in size and shape. Just as anticipatory, lots of 1-D nanostructures occurs in Fig. 6e,f by hydrothermally treating $Sr(NO_3)_2$, $Al(NO_3)_3 \cdot 9H_2O$, and $CO(NH_2)_2$ as 3:2:20 at 180 °C or 200 °C for 12 h, which clearly differ from those in Fig. 6a–d.

To arrest the intermediate states from the as-prepared precursors to final $Sr_3Al_2O_6$:Eu^{3+}, Dy^{3+} phosphor, a series of calcination temperature-dependent experiments were carried out in air. Fig. 7a shows us the typical FESEM image of the sample obtained by calcining the precursor prepared at 120 °C for 12 h

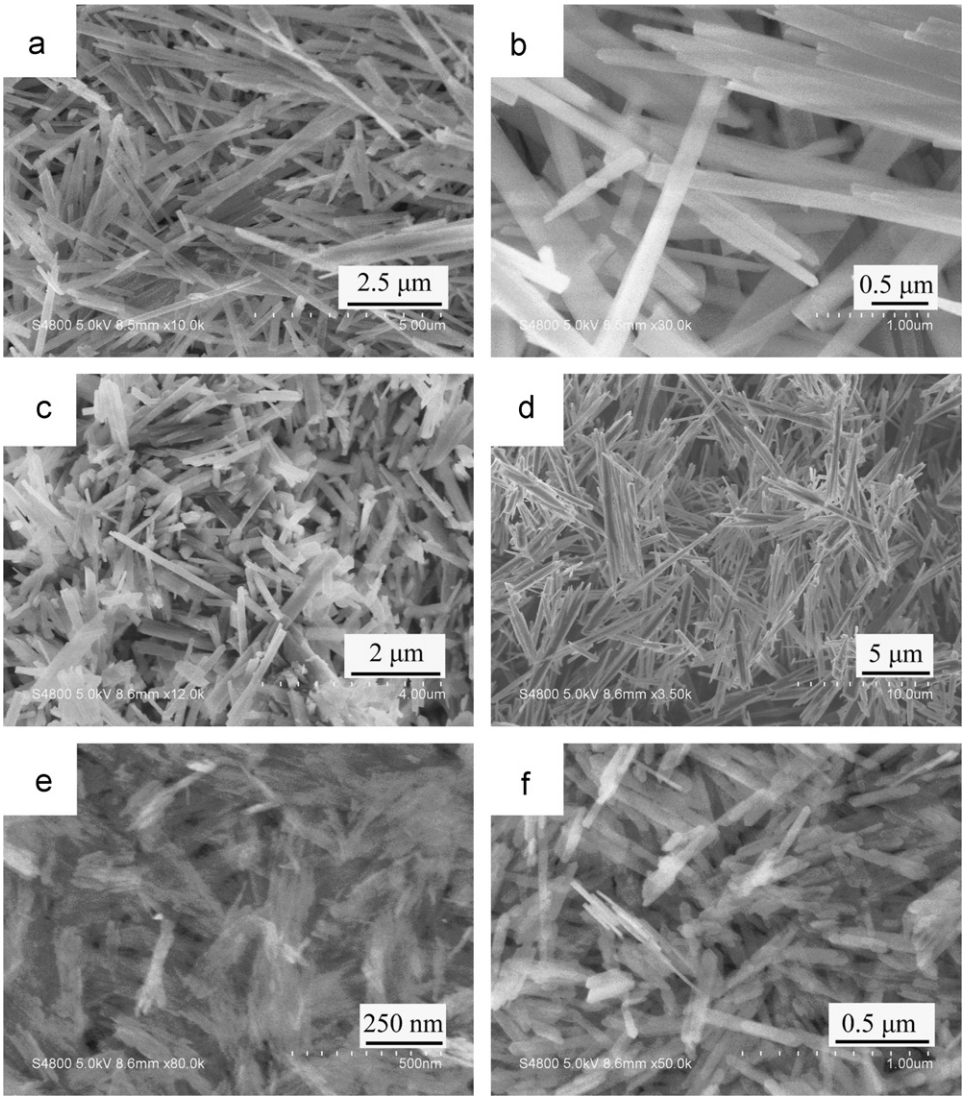

Fig. 6. FESEM images of samples acting as precursors obtained by keeping the mole ratio of $Sr(NO_3)_2$, $Al(NO_3)_3 \cdot 9H_2O$, and $CO(NH_2)_2$ as 3:2:20 at various reaction temperatures for 12 h: (a, b) 120 °C, (c) 140 °C, (d) 160 °C, (e) 180 °C, and (f) 200 °C.

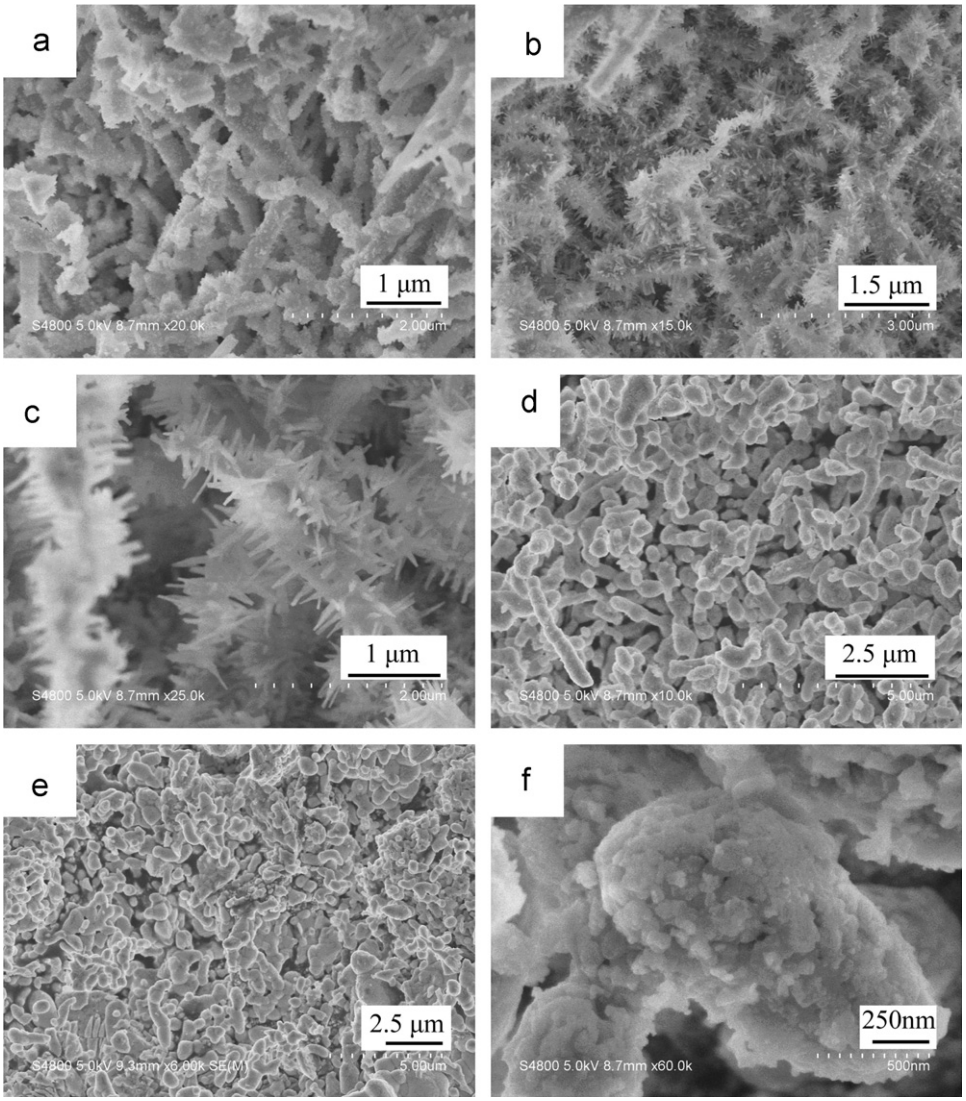

Fig. 7. FESEM images of samples obtained by calcining the precursor prepared at 120 °C for 12 h by keeping the mole ratio of $Sr(NO_3)_2$, $Al(NO_3)_3 \cdot 9H_2O$, and $CO(NH_2)_2$ as 3:2:20 at various temperatures in air for 3 h: (a) 900 °C, (b, c) 1000 °C, (d) 1100 °C, and (e, f) 1200 °C.

with mole ratio of $Sr(NO_3)_2$, $Al(NO_3)_3 \cdot 9H_2O$, and $CO(NH_2)_2$ as 3:2:20 at 900 °C in air. Clearly, the sample in Fig. 7a mainly consists of 1-D nanostructures, while large numbers of protrusions appear on their surfaces, unlike that of the precursor shown in Fig. 5a. When increasing the calcination temperature to 1000 °C, these protrusions turn into nanorods, forming novel hierarchical structures with branches perpendicularly growing along one trunk, as shown in Fig. 7b,c. However, when further increasing the calcination temperature to 1100 °C, these hierarchical structures vanish and a mass of imperfect nanorods appear in Fig. 7d, still remaining the 1-D nanostructures. Finally, $Sr_3Al_2O_6:Eu^{3+}$, Dy^{3+} phosphor possessing irregular shapes was obtained at the calcination temperature of 1200 °C in air for 3 h, as depicted in Fig. 7e,f. Hence, we find out that the higher calcination temperature is unfavorable for preparing $Sr_3Al_2O_6:Eu^{3+}$, Dy^{3+} phosphor having perfect 1-D nanostructures, which basically complies with our previous case of $MAl_2O_4:Eu^{2+}$, Dy^{3+} (M=Sr, Ba, Ca) phosphors [16].

Additionally, we conducted a series of calcination temperature-dependent experiments, ranging from 900 to 1200 °C, to prepare $Sr_3Al_2O_6:Eu^{2+}$, Dy^{3+} phosphor in a reducing atmosphere of H_2/Ar (20%+80%). As illustrated in Fig. 8, the shape evolution towards $Sr_3Al_2O_6:Eu^{2+}$, Dy^{3+} phosphor at various calcination temperatures mainly includes the transition from 1-D nanostructures to irregular particles. In other words, the lower calcination temperature favors the formation of 1-D nanostructures, while the higher favors the formation of irregular particles. Evidently, the shape evolution towards $Sr_3Al_2O_6:Eu^{2+}$, Dy^{3+} phosphor in Fig. 8 is analogous to that of $Sr_3Al_2O_6:Eu^{3+}$, Dy^{3+} phosphor shown in Fig. 7.

As is well known, the properties of nano- or micro-scale materials primarily depend on their shape and size. It is thus meaningful to manipulate these characteristics as we conceive. In this work, we obtained 1-D precursors in high yield when hydrothermally treating $Sr(NO_3)_2$, $Al(NO_3)_3 \cdot 9H_2O$, and $CO(NH_2)_2$ as 3:2:20 without any additives, as shown in Figs. 5 and 6. Next, certain amounts of sodium citrate were introduced into the above reaction system as a complexing agent to control the shape and size of samples. Fig. 9a shows the typical FESEM image of the sample obtained upon adding 10 mmol sodium citrate into the reaction system, mainly consisting of irregular particles while coexisting with minor amount of micro-meter quasi-spheres. Apparently, the shape and size of sample with sodium citrate as complexing agent differs from that obtained without sodium

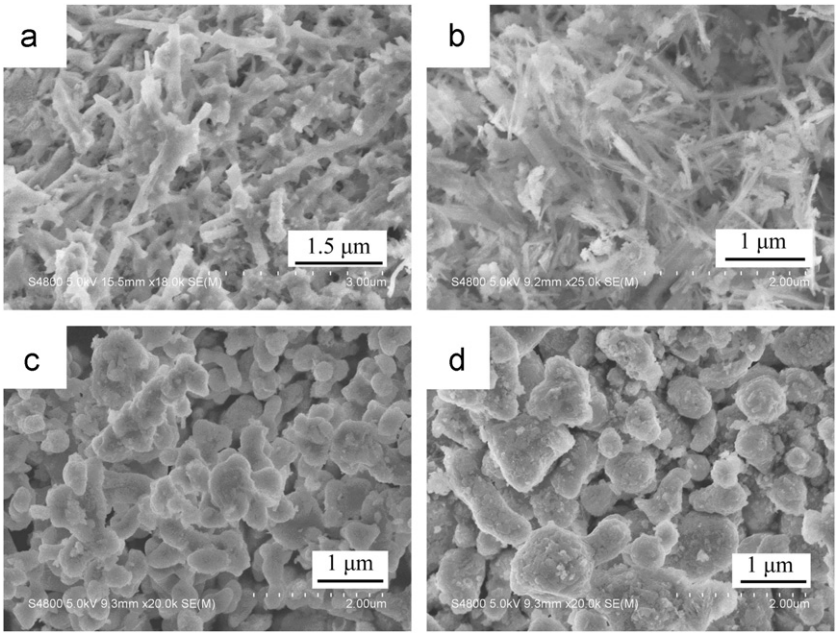

Fig. 8. FESEM images of samples obtained by calcining the precursor prepared at 120 °C for 12 h by keeping the mole ratio of $Sr(NO_3)_2$, $Al(NO_3)_3 \cdot 9H_2O$, and $CO(NH_2)_2$ as 3:2:20 at various temperatures in a reducing atmosphere of H_2/Ar (20%+80%) for 3 h: (a) 900 °C, (b) 1000 °C, (c) 1100 °C, and (d) 1200 °C.

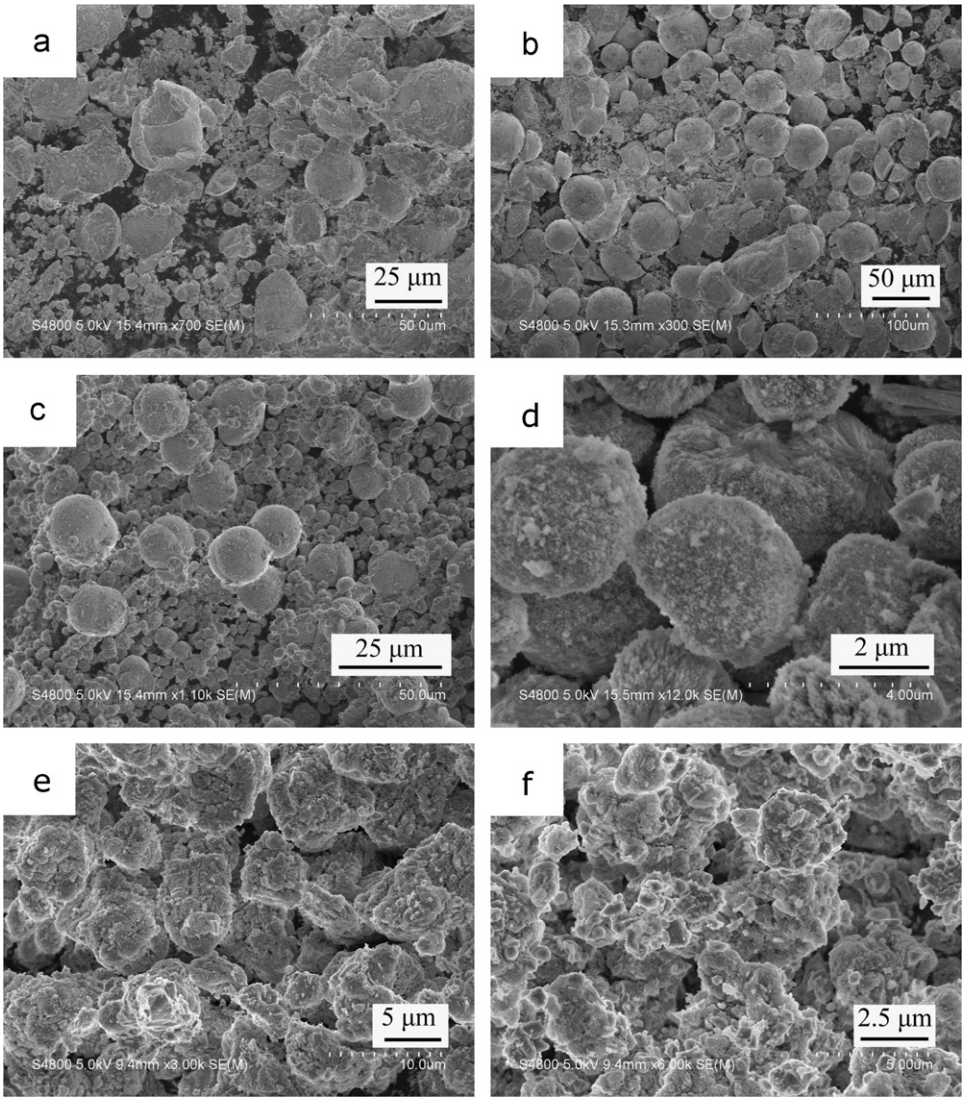

Fig. 9. FESEM images of samples acting as precursors obtained by hydrothermal treatment of $Sr(NO_3)_2$, $Al(NO_3)_3 \cdot 9H_2O$, and $CO(NH_2)_2$ as 3:2:20 at 120 °C for 12 h in the presence of various amounts of sodium citrate (mmol): (a) 10, (b) 20, and (c, d) 30. Next, the sample in figure (e, f) was calcined at 1200 °C for 3 h: (e) in air and (f) in a reducing atmosphere of H_2/Ar (20%+80%).

citrate. The FESEM image in Fig. 9a implies that the added sodium citrate has an important role in adjusting the shape and size in the reaction system containing $Sr(NO_3)_2$, $Al(NO_3)_3 \cdot 9H_2O$, and $CO(NH_2)_2$ as 3:2:20. In the following, when increasing the amount of sodium citrate added into the reaction system to 20 mmol, quasi-spheres in larger yielding appear, as revealed in Fig. 9b. Remarkably, large numbers of quasi-spheres with diameters ranging from several micrometers to tens of micrometers occur when adding 30 mmol sodium citrate into the reaction system, as depicted in Fig. 9c,d. Subsequently, the as-obtained quasi-spherical precursors in Fig. 9c,d were calcined at 1200 °C for 3 h in air or in a reducing atmosphere of H_2/Ar (20%+80%), which result in the formation of $Sr_3Al_2O_6$: Eu^{3+}, Dy^{3+} and $Sr_3Al_2O_6$: Eu^{2+}, Dy^{3+} phosphors, as shown in Fig. 9e,f, respectively. Besides, we can clearly see that the as-prepared $Sr_3Al_2O_6$: Eu^{3+} (Eu^{2+}), Dy^{3+} phosphors by adding sodium citrate are much larger than those phosphors obtained without adding sodium citrate.

The photoluminescence emission (PL) and photoluminescence excitation (PLE) spectra of the as-prepared $Sr_3Al_2O_6$:Eu^{3+}, Dy^{3+} were determined at room temperature. In the case of $Sr_3Al_2O_6$:Eu^{3+}, Dy^{3+} phosphors by adding 30 mmol sodium citrate, the typical excitation spectrum ranging from 250 to 550 nm at λ_{em}=589 nm is given in Fig. 10a_1. In detail, the broad band at ca. 260 nm derives from the charge transfer band between Eu^{3+} ions and the surrounding oxygen anions [18]. Concerning sharp bands centered at 525, 464, 393, and 362 nm can be ascribed to the characteristic transition of Eu^{3+} from $^7F_0 \rightarrow {}^5D_i$ (i=1, 2, 3, and 4). Additionally, Fig. 10b_1 depicts the typical red photoluminescence from Eu^{3+} ions in the $Sr_3Al_2O_6$:Eu^{3+}, Dy^{3+} phosphors when monitoring the excitation wavelength at 393 nm. A series of sharp bands at 577, 586, 619, 648, and 697 nm can be attributed to the characteristic transitions of Eu^{3+} from $^5D_0 \rightarrow {}^7F_j$ (j=0, 1, 2, 3, and 4). As for the case of $Sr_3Al_2O_6$: Eu^{3+}, Dy^{3+} phosphor without adding sodium citrate, similar PL and PLE spectra also exist, as shown in Fig. 10a_2 and b_2.

The excitation and emission spectra of $Sr_3Al_2O_6$: Eu^{2+}, Dy^{3+} phosphors obtained with or without adding sodium citrate were measured at room temperature. Fig. 11a shows the broad-band excitation spectra of Eu^{2+} ions in $Sr_3Al_2O_6$:Eu^{2+}, Dy^{3+} phosphors from 275 to 475 nm under various emission wavelengths. Meanwhile, Fig. 11b reveals the emission spectra of Eu^{2+} ions in $Sr_3Al_2O_6$:Eu^{2+}, Dy^{3+} phosphors from 460 to 750 nm under various excitation wavelengths, which all have the broad-band feature. In detail, Fig. 11b_1 is the emission spectrum centered at 489 nm under the excitation wavelength of 370 nm, which might come from the lattice host of $Sr_3Al_2O_6$. Besides, the red emission spectrum in Fig. 11b_2 centered at 606 nm under the excitation wavelength of 430 nm, belonging to the $4f^65d^1 \rightarrow 4f^7$ transition of Eu^{2+} ions in $Sr_3Al_2O_6$:Eu^{2+}, Dy^{3+} phosphors obtained by adding

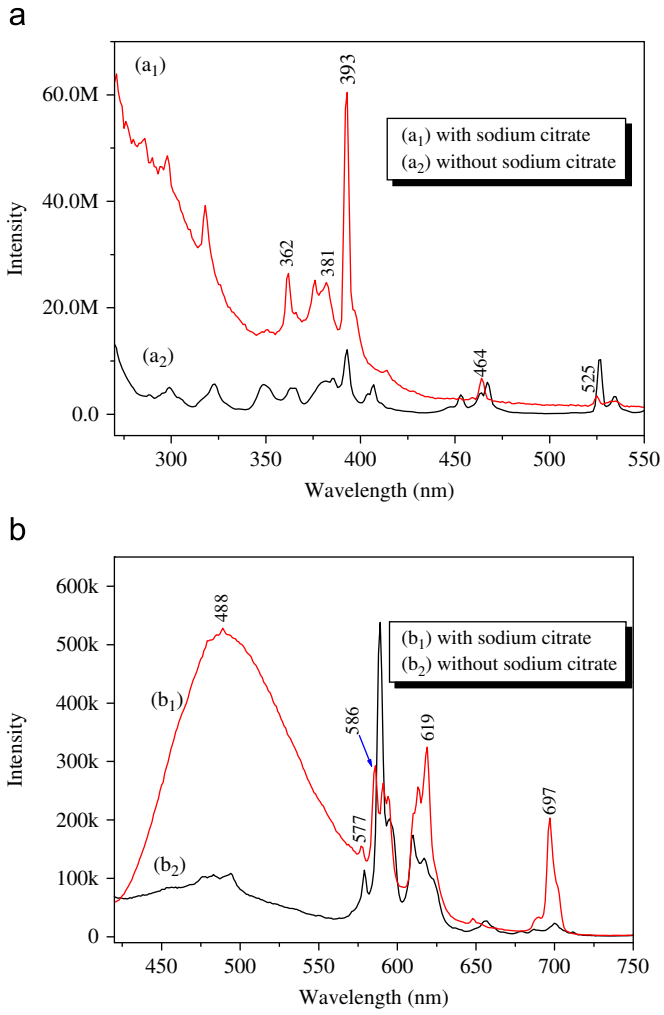

Fig. 10. (a) Excitation spectra of $Sr_3Al_2O_6$: Eu^{3+}, Dy^{3+} phosphors (λ_{em}=589 nm) with or without adding sodium citrate; (b) emission spectra of $Sr_3Al_2O_6$: Eu^{3+}, Dy^{3+} phosphors (λ_{ex}=393 nm) with or without adding sodium citrate.

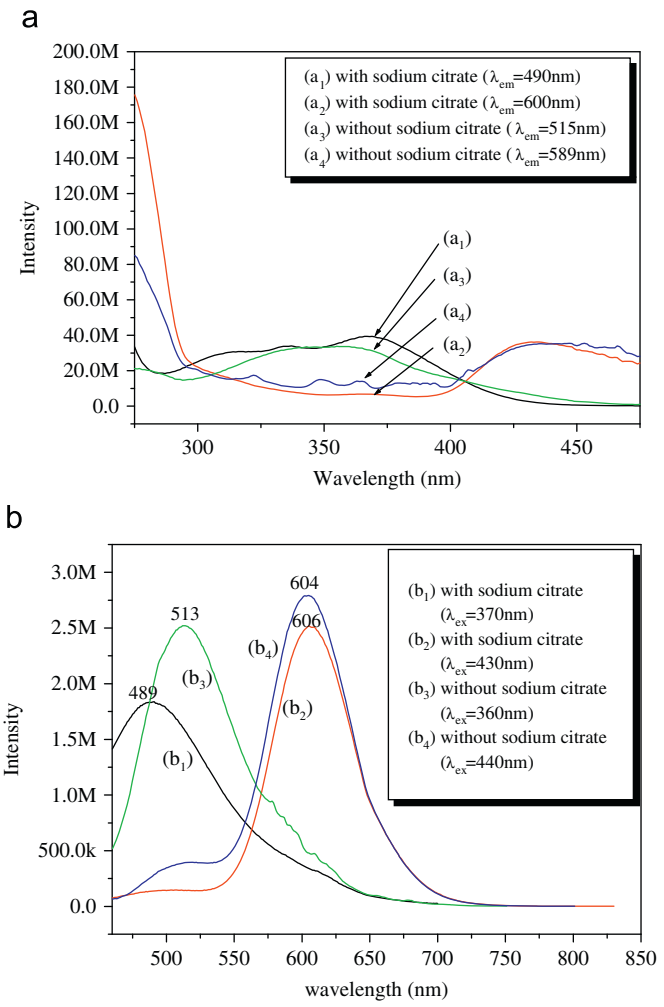

Fig. 11. (a) Excitation spectra of $Sr_3Al_2O_6$: Eu^{2+}, Dy^{3+} phosphors with or without adding sodium citrate; (b) emission spectra of $Sr_3Al_2O_6$: Eu^{2+}, Dy^{3+} phosphors with or without adding sodium citrate.

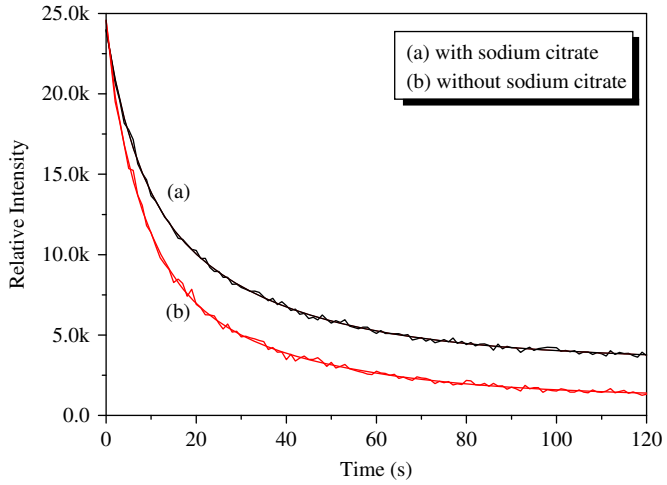

Fig. 12. Afterglow decay curves of phosphors after irradiating for 10 min: (a) $Sr_3Al_2O_6$: Eu^{2+}, Dy^{3+} obtained by adding sodium citrate using 430 nm xenon lamp as light source, (b) $Sr_3Al_2O_6$: Eu^{2+}, Dy^{3+} obtained without adding sodium citrate using 440 nm xenon lamp as light source.

sodium citrate [19]. As for the case of $Sr_3Al_2O_6$: Eu^{3+}, Dy^{3+} phosphors obtained without adding sodium citrate, analogous PL and PLE spectra occur in Fig. 11b_3 and b_4 under various excitation wavelengths.

Fig. 12 shows the decay curves of afterglow phosphorescence of $Sr_3Al_2O_6$: Eu^{2+}, Dy^{3+} phosphors, which were irradiated by using 440 and 430 nm xenon lamp as light source for 10 min, respectively. Clearly, all the afterglow decay curves are composed of two regimes, i.e., the initial rapid-decaying process and the subsequent slow-decaying process. As we know, Eu^{2+} ions are the luminescent centers and Dy^{3+} ions are the traps in aluminate phosphors. The long afterglow property usually results from the trap energy level produced by doping Eu^{2+} and Dy^{3+} ions in the crystals. The rapid-decaying process is due to the shore survival time of electron in Eu^{2+} and the slow-decaying process owes to the deep trap energy center of Dy^{3+} [20]. In addition, based on the following multiple exponential equations, we successfully fitted the decay carves [1]:

$$I = A_1 \exp\left(\frac{-t}{\tau_1}\right) + A_2 \exp\left(\frac{-t}{\tau_2}\right) + A_3 \exp\left(\frac{-t}{\tau_3}\right) \quad (1)$$

where I represents the phosphorescence intensity; A_1, A_2, and A_3 are constants; t is the time; τ_1, τ_2, and τ_3 are the decay times for the exponential components, respectively. Using the fitting function provided by Microsoft Origin, the parameters of τ_1, τ_2, and τ_3 are calculated and the corresponding results are given in Table 1. Obviously, the decay times of $Sr_3Al_2O_6$: Eu^{2+}, Dy^{3+} phosphor obtained by adding sodium citrate are much larger than those obtained without adding sodium citrate.

Table 1
Decay times for phosphorescence of $Sr_3Al_2O_6$: Eu^{2+}, Dy^{3+} samples.

Sample	Decay time (ms)		
	τ_1	τ_2	τ_3
With sodium citrate	22.15	6.23	49.02
Without sodium citrate	1.06	7.98	34.60

4. Conclusion

In summary, we present a simple and efficient hydrothermal treatment and subsequently postannealing approach to prepare $Sr_3Al_2O_6$: Eu^{2+} (Eu^{3+}), Dy^{3+} phosphors. It was found out that 1-D nanowires and quasi-spheres as precursors can be selectively prepared with or without adding sodium citrate, respectively, while their calcination products seem to be similar in shape. Besides, given the excitation spectrum, emission spectrum, and decay curve, the as-prepared $Sr_3Al_2O_6$: Eu^{2+} (Eu^{3+}), Dy^{3+} phosphors reveal excellent optical properties in nature. The findings reported in this work may open up new avenue for preparing aluminates phosphors with controlled structures and optical properties.

Acknowledgments

This project was supported by the Scientific Research Foundation for the Returned Overseas Chinese Scholars, Ministry of Education of China and Anhui Provincial Natural Science Foundation (090414194). The authors would gratefully thank Prof. Zheng Hua Wang at Anhui Normal University for his kind assistance.

References

[1] R. Sakai, T. Katsumata, S. Komuro, T. Morikawa, J. Lumin. 85 (1999) 149.
[2] C. Feldmann, et al., Adv. Funct. Mater. 13 (2003) 511.
[3] P.J. Saines, et al., J. Solid State Chem. 179 (2006) 613.
[4] W.Y. Jia, H.B. Yuan, L.Z. Lu, J. Lumin. 76 (1998) 424.
[5] B. Smets, J. Rutten, G. Hoeks, J. Electrochem. Soc. 136 (1989) 2119.
[6] T. Matsuzawa, Y. Aoki, N. Takeuchi, J Electrochem. Soc. 143 (1996) 2670.
[7] T. Katsumata, K. Sasajima, T. Nabae, J. Am. Ceram. Soc. 81 (1998) 413.
[8] T. Aitasalo, P. Deren, et al., J. Solid State Chem. 171 (2003) 114.
[9] Y. Liu, C.N. Xu, J. Phys. Chem. B 107 (2003) 3991.
[10] A. Nag, T.R.N. Kutty, J. Alloys Compd. 354 (2003) 221.
[11] Y. Lin, Z. Zhang, Z. Pang, et al., Chem. Phys. 70 (2001) 156.
[12] T. Peng, L. Huajun, H. Yang, C. Yan, Mater. Chem. Phys. 85 (2004) 68.
[13] Y. Lin, Z. Tang, Z. Zhang, Mater. Lett. 51 (2001) 14.
[14] P.D. Sarkisov, N.V. Popovich, A.G. Zhelnin, Glass Ceram. 60 (2003) 309.
[15] Y.B. Xu, Y.Y. He, X. Yuan, Powder Technol. 172 (2007) 99.
[16] X.Y. Chen, C. Maet al., J. Phys. Chem. C 113 (2009) 2685.
[17] X.Y. Chen, H.S. Huh, S.W. Lee, Nanotechnology 18 (2007) 285608 (5pp).
[18] B.S. Barros, P.S. Melo, et al., J. Mater. Sci. 41 (2006) 4744.
[19] P. Zhang, M.X. Xu, Z.T. Zheng, et al., J. Sol-Gel Sci. Technol. 43 (2007) 59.
[20] T. Katasumata, T. Nabae, K. Sasajima, et al., J. Crystal Growth 183 (1998) 361.